Available online at www.sciencedirect.com
SCIENCE DIRECT®
Journal of Nuclear Materials 344 (2005) 206–212
journal of nuclear materials
www.elsevier.com/locate/jnucmat

Thermodynamic and kinetic aspects of UO_2 fuel oxidation in air at 400–2000 K

Peter Taylor *

Institut de Radioprotection et de Súreté Nucléaire, Direction de la Prévention des Accidents Majeurs, Centre de Cadarache, B.P. 3, 13115 St. Paul lez Durance, France

Abstract

Most nuclear fuel oxidation research has addressed either low-temperature (<700 K) air oxidation related to fuel storage or high-temperature (>1500 K) steam oxidation linked to reactor safety. This paper attempts to unify modelling for air oxidation of UO_2 fuel over a wide range of temperature, and thus to assist future improvement of the ASTEC code, co-developed by IRSN and GRS. Phenomenological correlations for different temperature ranges distinguish between oxidation on the scale of individual *grains* to U_3O_7 and U_3O_8 below ~700 K and individual *fragments* to U_3O_8 via UO_{2+x} and/or U_4O_9 above ~1200 K. Between about 700 and 1200 K, empirical oxidation rates slowly decline as the U_3O_8 product becomes coarser-grained and more coherent, and fragment-scale processes become important. A more mechanistic approach to high-temperature oxidation addresses questions of oxygen supply, surface reaction kinetics, thermodynamic properties, and solid-state oxygen diffusion. Experimental data are scarce, however, especially at low oxygen partial pressures and high temperatures.

1. Introduction

Some severe accident scenarios involve access of air to a degraded reactor core in the later stages of the accident sequence. One possible consequence is that the UO_2 fuel is oxidized sufficiently for a significant release of ruthenium, which is an important fission product from a radiological safety viewpoint. It is therefore important to understand the kinetics of UO_2 oxidation, the oxygen potential distribution within the fuel, and the thermochemistry of the Ru–O system under such conditions. This study was performed to help define conditions for a possible future Phébus test [1,2], and in the longer term to improve UO_2 oxidation modelling in the ASTEC code, which is being co-developed by the French Institute for Radiological Protection and Nuclear Safety (IRSN) and the German Gesellschaft für Anlagen- und Reaktorsicherheit (GRS). While oxidation of the hottest portion of the fuel ($\geqslant$2000 K) is of primary importance, the possibility of U_3O_8 powder formation in cooler portions of the fuel is also of interest.

2. The U–Ru–O system

To help understand the changes in oxidation behaviour with increasing temperature, a simplified phase diagram is shown in Fig. 1. This is based on phase-transition temperatures estimated by Guéneau et al. [3] in

* Present address: P.O. Box 597, Pinawa, Manitoba R0E 1L0, Canada. Tel.: +1 204 753 2977.
E-mail address: taylorp@granite.mb.ca

0022-3115/$ - see front matter © 2005 Elsevier B.V. All rights reserved.
doi:10.1016/j.jnucmat.2005.04.043

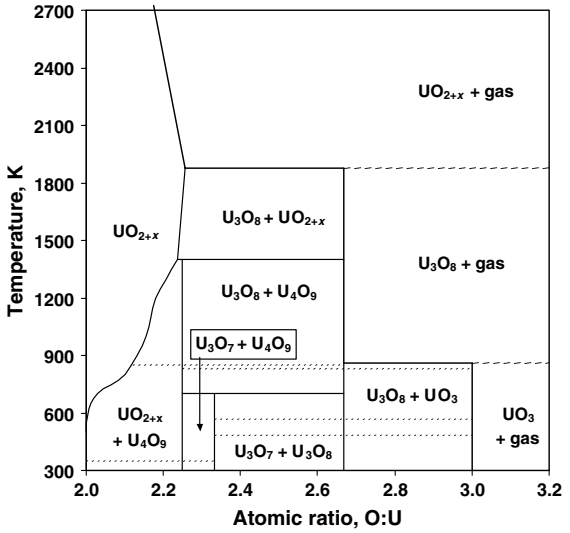

Fig. 1. Simplified portion of the U–O phase diagram, emphasizing solid phases with compositions between UO_2 and UO_3. The diagram is based mainly on Table 1 and Fig. 2 of Guéneau et al. [3]. The five horizontal, dotted lines represent solid phase transitions in U_4O_9 at 348 and 850 K, and in U_3O_8 at 483, 568, and 830 K. The dashed lines at 861 and 1878 K represent the decomposition of UO_3 and U_3O_8, respectively, in air.

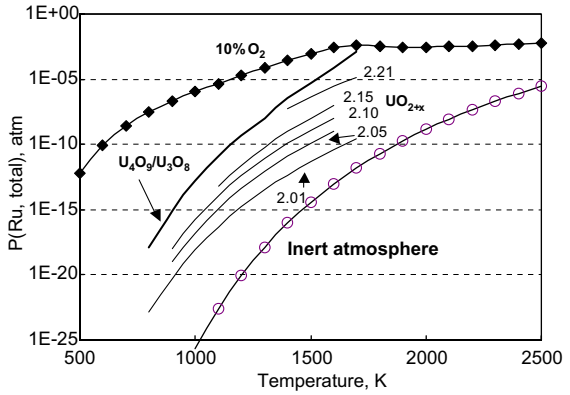

Fig. 2. Calculated total ruthenium vapour pressure (sum of all RuO_n species) under various conditions. The numbers 2.01, 2.05, etc., are values of $2 + x$ in UO_{2+x}.

their recent review of U–O thermodynamics. While Fig. 1 includes the temperature–composition (T–C) boundary for UO_{2+x}, both U_4O_9 and U_3O_8 are treated as stoichiometric phases, because their stoichiometric limits (U_4O_{9-y} and U_3O_{8-z}) are less well characterized [3–7].

Some of the higher oxides are inaccessible for kinetic reasons at low temperatures, and for thermodynamic reasons at high temperatures. Thus, dry oxidation of UO_2 normally ceases at U_3O_8 even when UO_3 is stable in air [3,8], and formation of U_3O_8 itself is very slow below ~500 K [8–10]. The evaluated thermal stability limit of U_3O_8 in air is 1878 K [3]. It remains uncertain whether U_3O_7 is metastable or marginally stable below ~700 K; thermodynamic data from Grenthe et al. [11] indicate that it is stable with respect to disproportionation, Eq. (1), by just 0.7 ± 2.0 kJ (mol U)$^{-1}$ at 298 K:

$$5U_3O_7 = U_3O_8 + 3U_4O_9 \quad [UO_{2.333} = 0.2UO_{2.667} + 0.8UO_{2.250}]. \tag{1}$$

While the effects of burnup or irradiation on fuel oxidation kinetics are generally small, the distinction between U_4O_9, U_3O_7 and UO_{2+x} becomes blurred at moderate to high burnups, at least partly because dissolved fission products and actinides disrupt the long-range ordering of oxygen atoms (defect clusters) that distinguishes U_4O_9 and U_3O_7 [8,9]. Fission products also inhibit U_3O_8 formation, apparently because many of them (notably the lanthanides) are much less soluble in U_3O_8 than in UO_2 [9,12,13]. The formation of U_3O_8 may also be inhibited by its high radiation sensitivity relative to UO_{2+x} [14].

Fig. 2 shows the calculated vapour pressure of ruthenium (sum of all RuO_n species, $0 \leqslant n \leqslant 4$) under different redox conditions, mostly corresponding to different uranium oxide compositions. The calculations – which assume unit activity of Ru(s) or RuO_2(s), whichever is stable[1] – are based on ruthenium oxide data from Garisto [15] and Cordfunke and Konings [16], and UO_{2+x} correlations from Labroche et al. [6]. The figure illustrates the importance of attaining a high degree of fuel oxidation before significant ruthenium release can occur (this requires $p(\mathrm{Ru,total}) > \sim 10^{-5}$ atm).

3. Phenomenological modelling

This approach is based on recent reviews of U_3O_7 and U_3O_8 formation from UO_2 powder or fuel below 700 K, and a small number of publications for higher temperature oxidation. Most of the published data applies to 'unlimited air' conditions, with very limited information at low $p(O_2)$ values, therefore the equations provide upper limits to oxidation rates for conditions of limited air access.

3.1. Formation of U_3O_7 below 700 K

McEachern [17] reviewed UO_2 powder oxidation and recommended Eq. (2), where the 'parabolic' rate

[1] The thermal stability limit for RuO_2(s) varies with T and $p(O_2)$, and is about 1700 K in air.

constant, k_1, describes growth of a U_3O_7 layer of thickness τ on UO_2 in air at 398–623 K, consistent with rate control by oxygen diffusion through a thickening product layer:

$$\ln(k_1, \mathrm{m^2\ s^{-1}}) = \frac{-95.7\ \mathrm{kJ\ mol^{-1}}}{RT} - 17.33 = \frac{-11510}{T} - 17.33, \quad (2)$$

where

$$\tau(\mathrm{m}) = (k_1 t)^{0.5}. \quad (3)$$

The fractional conversion, $\alpha_{U_3O_7}$, for spherical particles of radius r, is obtained by using either the Jander approximation, Eq. (4), or the more accurate Ginstling–Brounshtein (GB) Eq. (5), where a is the ratio of the molar volumes of U_3O_7 and UO_2 (0.97 for β-U_3O_7) [18,19]:

$$\tau = a \cdot r(1 - (1 - \alpha_{U_3O_7})^{1/3}) = (k_1 t)^{0.5}, \quad (4)$$

$$1 - \frac{2\alpha_{U_3O_7}}{3} - (1 - \alpha_{U_3O_7})^{2/3} = \frac{k_1 t}{a^2 \cdot r^2}. \quad (5)$$

In irradiated LWR fuel, oxidation penetrates individual fragments along the grain boundaries to produce a layer of cubic 'U_4O_{9+y}' (as opposed to tetragonal U_3O_7) on individual grains [20–22]. Partial grain separation, plus some intragranular cracking, arises from the 2% volume reduction associated with this oxidation step, and enhances gaseous access for further oxidation. The burnup effect on oxygen consumption appears to be small [17], and Eqs. (2)–(5) thus seem quite robust, but several points should be borne in mind. Firstly, the diffusion mechanism in U_4O_9/U_3O_7 is not understood in detail. Desgranges et al. [23] recently showed that U_4O_9 as well as U_3O_7 is produced in UO_2 oxidation near 523 K, implying a more complex diffusion–reaction sequence. There is also evidence for a linear kinetic regime under some conditions, implying rate control by interfacial reaction kinetics rather than diffusion [17]; this is most clearly demonstrated in single-crystal oxidation near 450 K [24]. Finally, grain-boundary oxidation in irradiated fuel is not always uniform [22,25], and there is sometimes an oxidation front within a fuel fragment.

3.2. Formation of U_3O_8 below 700 K

This reaction is commonly described as a nucleation-and-growth process [8]; in one recent attempt to describe the kinetics, McEachern et al. [10] obtained Eq. (6) and the truncated Eq. (7) for U_3O_8 formation, based on data for surface oxidation of unirradiated CANDU fuel:

$$\ln(k_2, \mathrm{h^{-3}}) = \frac{-52\,808 \pm 3442}{T} + 86.165, \quad (6)$$

$$\alpha_{U_3O_8} \cong 1 - \exp\left(\frac{-\pi \cdot k_2 \cdot t^3}{3}\right). \quad (7)$$

Eq. (7) is a variant of the well-known, empirical Avrami equation. The numerator in Eq. (6) corresponds to an apparent activation energy, $E_2 = 146\ \mathrm{kJ\ mol^{-1}}$ (averaged over the nucleation-and-growth steps), in good agreement with the value of $154\ \mathrm{kJ\ mol^{-1}}$ obtained by a critical literature review [8].

Eqs. (6) and (7) were developed to estimate time–temperature limits for the onset of U_3O_8 formation below 500 K, based mainly on data obtained at 500–600 K. Caution is necessary in applying these equations to higher temperatures and/or high degrees of conversion, for several reasons.

Perhaps most important, the nucleation-and-growth processes are not deconvoluted; Kolář [26] has shown how to separate these processes mathematically, but only for the somewhat artificial two-dimensional (2D) case. In fact, Eq. (7) is a 2D model derived from 3D X-ray diffraction data, albeit biased towards the outermost 1-μm surface layer [10,27]. While it produces the expected sigmoidal oxidation curves for U_3O_8 formation, it tends to overestimate the rates at high conversion ($\alpha_{U_3O_8} > 0.5$), likely because the constant radial growth rate is constrained only by the intersection of growing nuclei, with no allowance for other growth-terminating or -limiting mechanisms.

Formation of U_3O_8 is markedly inhibited with increasing burnup, at least in part by fission or activation products in solid solution in the UO_2 [8–10,13,28,29]. The value of k_2 should therefore be modified by a burnup parameter. Eq. (7) should also include a grain-size term to represent variation in the density of nucleation sites with grain-surface area (grains are separated by the U_3O_7 step, see Section 3.1). Furthermore, oxygen supply (mass balance) may become rate-limiting above ~600 K [30]. Finally, above about 800 K, powder formation is curtailed by the gradual transition from grain-scale to fragment-scale kinetics, as described below.

Thus, for present purposes, Eqs. (6) and (7) provide a 'flag' for potential runaway powder formation near 700 K, rather than a quantitative model.

3.3. Formation of U_4O_9 and U_3O_8 at 700–1200 K

Peakall and Antill [31] and McCracken [32] reported a gradual *decrease* in the overall oxidation rate of UO_2 pellets with increasing temperature between about 700 and 1200 K. This can be explained by a gradual change-over from rate control at the level of individual grains (with powder formation) below 700 K to that of individual fragments (which remain intact) above 1200 K. Rates are erratic, due to occasional breakaway of oxidation products from the fragment surface, but

approximately linear kinetics were observed. The reported rates at 723–1173 K, measured after 30% oxidation to U_3O_8 [31], yield Eq. (8):

$$k_3(\text{mol O}_2\ \text{m}^{-2}\ \text{s}^{-1}) = 0.01095 - 8.524 \times 10^{-6} T. \quad (8)$$

This equation provides an empirical 'bridge' between the phenomenological expressions for oxidation below 700 K (Sections 3.1 and 3.2) and above 1200 K (Section 3.4).

McCracken [32] also found that the overall oxidation rate declined, from a maximum near 770 K (>90% conversion to U_3O_8 in 1 h) to a minimum near 1270 K (<75% conversion in 10 h). At 970 and 1070 K, the product was a partly protective mat of microcrystalline U_3O_8, quite different from the fine powder produced around 700 K. Above ~1200 K, the U_3O_8 layer was sufficiently coherent (relatively large, columnar grains) to become a rate-controlling barrier.

3.4. Formation of UO_{2+x} or U_4O_9, and U_3O_8, above 1200 K

Extending McCracken's study, Cox et al. [33] measured the thickness of U_3O_8, and estimated the quantity of underlying U_4O_9 or UO_{2+x} (see Fig. 1) formed on UO_2 disks in air at 1173–1473 K. Their results yield Eq. (9) for U_4O_9/UO_{2+x} and Eq. (10) for U_3O_8 formation:

$$\ln(k_4, \text{m}^2\ \text{s}^{-1}) = \frac{-22\,300}{T} - 2.36, \quad (9)$$

$$\ln(k_5, \text{m}^2\ \text{s}^{-1}) = \frac{-20\,700}{T} - 8.20. \quad (10)$$

The corresponding activation energies of ~185 and ~170 kJ mol^{-1} are not significantly different, and the controlling step for both phases is likely oxygen diffusion through the outer layer of U_3O_8. However, the diffusion properties of U_3O_8 are not well enough known to test this hypothesis. The parabolic rate constants k_4 and k_5 can be related to the product layer thickness τ, as described for k_1 in Section 3.1.

Because of the diverse types of kinetic expression (one linear, three parabolic and one sigmoidal), as well as the switch from grain-scale to fragment-scale oxidation, it is difficult to compare the rate constants in Eqs. (2), (6), and (8)–(10). Fig. 3 shows the oxygen consumption rates for the five processes, based on spherical fragments with a radius of 1 mm and grain-radius of 5 μm, all at either 5% (Fig. 3(a)) or 30% completion (Fig. 3(b)). It illustrates the following points: (a) formation of U_3O_7 is important only at low temperatures and short reaction times, and is overtaken by U_3O_8 formation at ~700 K; (b) runaway formation of U_3O_8 at the grain level above ~700 K is 'reined in' as the oxidation changes from grain-level to fragment-level control (Peakall–Antill kinetics); (c) diffusion-controlled formation of U_4O_9/UO_{2+x} and U_3O_8 become important above ~1000 K.

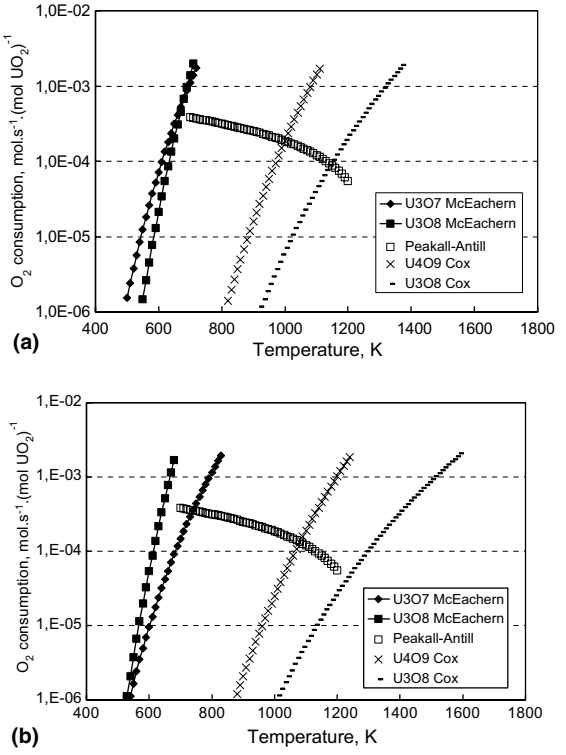

Fig. 3. Relative oxygen consumption rates at (a) 5% and (b) 30% completion for the five oxidation processes, calculated for spherical fuel fragments, r = 1 mm, grain radius = 5 μm.

Extrapolation of Eqs. (9) and (10) is invalid beyond the thermal stability limit of U_3O_8 (~1878 K in air, see Fig. 1), because they are related to diffusion through a U_3O_8 layer. In fact, the extrapolation appears to overpredict the oxidation rates. For example, Eqs. (9) and (5), substituting $\alpha_{UO_{2+x}}$ for $\alpha_{U_3O_7}$, predict reaction times of ~1 s for complete oxidation of 1-mm-radius spheres of UO_2 to UO_{2+x} near 1800 K. This is inconsistent with the reported 250-s delay in ruthenium release from CANDU fuel fragments in air at 1873 K [34], which is probably due to a combination of kinetic and oxygen-transport limitations on the fuel oxidation.

4. Mechanistic modelling requirements near 2000 K

Following a similar approach to Olander's steam-oxidation model [35], high-temperature air oxidation can be described by three groups of basic processes (in addition to gas-phase mass transport of O_2 and UO_3).

A. *Reaction* of O_2 at the oxide surface; the flux to the surface may be modified by additional reactions of O, OH and H_2O, plus condensation of UO_3.
B. *Evaporation* of O_2 and UO_3 from the oxide surface.
C. *Chemical diffusion* of oxygen into the specimen (down the oxygen potential gradient in UO_{2+x}).

The flux in a finite surface element for Process A, which can be expressed as an oxygen sticking coefficient, is balanced by the fluxes for Processes B and C. In general, during oxidation, the instantaneous surface composition is poised below the equilibrium value of x. At the equilibrium UO_{2+x} composition for any given $p(O_2)$ value, the flux for Process C falls to zero, and those for Processes A and B are equal and opposite.

4.1. T–C–p(O2) relationships

Key pre-requisites for developing a model include high-temperature T–C–$p(O_2)$ and T–C–D relationships for UO_{2+x} (D = diffusion coefficient). The T–C range lies beyond that of published UO_{2+x} research, except a study by Anthony et al. [36], who obtained the following empirical correlation for compositions near the UO_{2+x}–U_3O_{8-y} phase boundary:

$$\ln p(O_2) = 70x - \frac{32\,900}{T} - 1.05. \tag{11}$$

The T–C–$p(O_2)$ relationship can also be estimated from the series of correlations of the form $\log_{10}p(O_2) = \frac{A}{T} + B$ (for $0.01 < x < 0.23$, and mostly for $900\ \mathrm{K} < T < 1600\ \mathrm{K}$) provided by Labroche et al. [6]. These correlations yield the following empirical expressions, valid only for $0.05 < x < 0.25$:

$$\log_{10}p(O_2) = x\left(\frac{-4026.8}{T} + 22.015\right) - \frac{14941}{T} + 1.999, \tag{12}$$

$$x(\text{limiting value in air}) = \frac{787.96}{T} - 0.15404, \tag{13}$$

$$\frac{\mathrm{d}(\overline{G}(O_2), \mathrm{kJ\ mol^{-1}})}{\mathrm{d}x} = 0.42145T - 77.09. \tag{14}$$

Extrapolation of Eq. (12) to 1600–2000 K (Fig. 4) yields results similar to Kim's recent correlations [5], but only fair agreement with the earlier Lindemer–Besmann model [37], and poor agreement with Eq. (11).

4.2. Rate control: surface reaction or oxygen diffusion?

Current models for steam oxidation of UO_2 are based on the well-founded assumption that oxygen diffusion in the fuel is relatively fast, and that surface reaction kinetics are rate-determining [35,38]. This is not necessarily the case for air oxidation, where surface reaction rates are likely higher than with steam, and relatively slow diffusion at high values of x may become important in the later stages of oxidation (a key stage before ruthenium release, see Section 2).

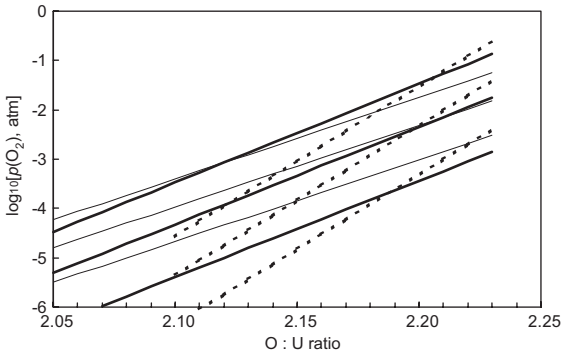

Fig. 4. T–C–$p(O_2)$ relationships at 2000 K (uppermost lines), 1800 K and 1600 K, according to Anthony et al. [36] (bold, dashed lines; Eq. (11)), Lindemer and Besmann [37] (faint, solid lines), and extrapolation from Labroche et al. [6] (bold, solid lines; Eq. (12)).

A lower limit for the oxygen sticking coefficient associated with Process A can be estimated from the observed uranium evaporation rate from UO_{2+x} (oxidized fuel, $x \sim 0.24$) of $\sim 10^{-4}\ \mathrm{g\ cm^{-2}\ s^{-1}}$ in air near 2000 K [39]. The corresponding oxygen reaction rate, based on Eq. (15) is $\sim 1.5 \times 10^{-4}\ \mathrm{g\ cm^{-2}\ s^{-1}}$, which corresponds to a minimum sticking coefficient (i.e., ignoring oxygen evaporation) of $\sim 4 \times 10^{-6}$ (on $UO_{2.24}$ at 2000 K).[2]

$$UO_{2+x}(s) + \left(\frac{1-x}{2}\right)O_2(g) = UO_3(g). \tag{15}$$

Ruello et al. [40] have recently shown that the chemical diffusion coefficient for oxygen in UO_{2+x} is strongly dependent on x. Extrapolation of their results, obtained at 973–1673 K, indicates diffusion coefficients near $10^{-5}\ \mathrm{cm^2\ s^{-1}}$ for $x < 0.03$, and $10^{-6}\ \mathrm{cm^2\ s^{-1}}$ for $0.07 < x < 0.17$, at 2000 K. They reported 'sluggish' response in attempted measurements at still higher values of x.

As noted above, Hunt et al. [34] reported a 250-s delay in ruthenium release from CANDU fuel fragments in air at 1873 K. The four fragments had a mass of 0.69 g, corresponding to an equivalent spherical radius of 0.155 cm. Using the Booth approximation, Eq. (16), the time t for oxidation to proceed from fractional conversion (UO_2 to UO_{2+x}) $f = 0$ to 0.1, and from 0.8 to 0.9,

[2] Based on a collision rate of $\frac{44.33}{\sqrt{MT}}\ \mathrm{mol\ cm^{-2}\ s^{-1}}$ for a pure gas of molecular weight M at temperature T (K) at atmospheric pressure, derived from standard kinetic expressions for an ideal gas.

Table 1
Hypothetical, diffusion-controlled reaction times dt, and equivalent oxygen sticking coefficients S, for given values of D, r, f_1 and f_2

D (cm^2 s^{-1})	r (cm)	f_1	f_2	d$t = t_2 - t_1$ (s)	S
10^{-5}	0.155	0	0.1	2.2	3×10^{-4}
10^{-5}	0.155	0.8	0.9	169.2	4×10^{-6}
10^{-6}	0.155	0.8	0.9	1692	4×10^{-7}
10^{-5}	0.05	0	0.1	0.23	3×10^{-3}
10^{-5}	0.05	0.8	0.9	17.6	4×10^{-5}
10^{-6}	0.05	0.8	0.9	176	4×10^{-6}

can be estimated for given values of diffusion coefficient D and fragment radius r [41]:

$$f = 6\left(\frac{Dt}{\pi r^2}\right)^{1/2} - \frac{3Dt}{r^2}. \quad (16)$$

Table 1 shows representative calculations for different values of D and r. These indicate that, for diffusion to be sufficiently fast to match an oxygen sticking coefficient of 4×10^{-6}, between 80% and 90% completion, the diffusion coefficient should be $\sim10^{-6}$ cm^2 s^{-1} for $r = 0.05$ cm and $\sim10^{-5}$ cm^2 s^{-1} for $r = 0.155$ cm. Thus, while surface reaction kinetics is likely to be rate-controlling in the early stages of oxidation, oxygen diffusion may become rate-limiting in the later stages.

The situation is made more complex above ~2000 K, under conditions favouring uranium volatilization, by the development of a highly porous microstructure [42]. This implies a reversion to grain-scale oxidation and diffusion; presumably gaseous diffusion and surface reaction kinetics become rate-limiting in this case.

5. Conclusions

Many of the differences in air-oxidation kinetics of UO_2 fuel between 400 and 1500 K are linked to changing microstructure of the U_3O_8 product, as well as differences in the intermediate product(s), namely U_3O_7, U_4O_9, and UO_{2+x}. Above the stability limit of U_3O_8 (~1878 K in air), UO_{2+x} is the sole oxidation product, the limiting value of x declining slowly with increasing temperature. Oxidation at temperatures near 2000 K is likely controlled by surface reaction kinetics in the early stages and by oxygen diffusion in the late stages.

References

[1] M. Schwarz, G. Hache, P. von der Hardt, Nucl. Eng. Design 187 (1999) 47.
[2] B. Clément, N. Hanniet-Girault, G. Repetto, D. Jacquemain, A.V. Jones, M.P. Kissane, P. von der Hardt, Nucl. Eng. Design 226 (2003) 5.
[3] C. Guéneau, M. Baichi, D. Labroche, C. Chatillon, B. Sundman, J. Nucl. Mater. 304 (2002) 161.
[4] P.-Y. Chevalier, E. Fischer, B. Cheynet, J. Nucl. Mater. 303 (2002) 1.
[5] Y.S. Kim, J. Nucl. Mater. 279 (2000) 173.
[6] D. Labroche, O. Dugne, C. Chatillon, J. Nucl. Mater. 312 (2003) 21.
[7] D. Labroche, O. Dugne, C. Chatillon, J. Nucl. Mater. 312 (2003) 50.
[8] R.J. McEachern, P. Taylor, J. Nucl. Mater. 254 (1998) 87.
[9] J.W. Choi, R.J. McEachern, P. Taylor, D.D. Wood, J. Nucl. Mater. 230 (1996) 250.
[10] R.J. McEachern, J.W. Choi, M. Kolář, W. Long, P. Taylor, D.D. Wood, J. Nucl. Mater. 249 (1997) 58.
[11] I. Grenthe, J. Fuger, R.J.M. Konings, R.J. Lemire, A.B. Muller, C. Nguyen-Trung, H. Wanner, Chemical Thermodynamics of Uranium, NEA/OECD and North-Holland, 1992.
[12] R.J McEachern, D.C. Doern, D.D. Wood, J. Nucl. Mater. 252 (1998) 145.
[13] G.-S. You, K.-S. Kim, D.-K. Min, S.-G. Ro, J. Nucl. Mater. 277 (2000) 325.
[14] Hj. Matzke, J.L. Whitton, Can. J. Phys. 44 (1966) 995.
[15] F. Garisto, Atomic Energy of Canada Limited Report, AECL-9552, 1988.
[16] E.H.P. Cordfunke, R.J.M. Konings, Thermochemical Data for Reactor Materials and Fission Products, North-Holland, 1990.
[17] R.J. McEachern, J. Nucl. Mater. 245 (1997) 238.
[18] S. Aronson, R.B. Roof Jr, J. Belle, J. Chem. Phys. 27 (1957) 137.
[19] L.G. Harrison, Compr. Chem. Kinet. 2 (1969) 377.
[20] R.E. Einziger, L.E. Thomas, H.C. Buchanan, R.B. Stout, J. Nucl. Mater. 190 (1992) 53.
[21] L.E. Thomas, R.E. Einziger, Mater. Charact. 28 (1992) 149.
[22] L.E. Thomas, O.D. Slagle, R.E. Einziger, J. Nucl. Mater. 184 (1991) 117.
[23] L. Desgranges, G. Rousseau, J.-C. Niepce, J.-F. Berar, G. Baldinozzi, MRS Fall 2003 Meeting, Boston, MA, Paper DD1.2.
[24] F. Garrido, L. Thomé, J.-M. Gras, S. Klaumünzer, in: Proceedings of the 8th International Conference on Radioactive Waste Management and Environmental Remediation (ICEM'01), Bruges, Belgium, 2001, Session 10, Paper 5.
[25] L. Desgranges, S. Kloepfer, G. Eminet, J. Noirot, P. Drevon, V. Broudic, A. Bérès, in: Proceedings of the 8th International Conference on Radioactive Waste Management and Environmental Remediation, Bruges, Belgium, 30 September–4 October 2001.
[26] M. Kolář, J. Nucl. Mater. 301 (2002) 210.
[27] P. Taylor, E.A. Burgess, D.G. Owen, J. Nucl. Mater. 88 (1980) 153.
[28] B.D. Hanson, Pacific Northwest National Laboratory Report, PNL-11929, 1998.
[29] K.-S. Kim, G.-S. You, D.-K. Min, S.-G. Ro, E.-K. Kim, J. Kor. Nucl. Soc. 29 (1997) 93.
[30] I.J. Hastings, D.H. Rose, J.R. Kelm, D.A. Irvine, J. Am. Ceram. Soc. 69 (1986) C-16.
[31] K.A. Peakall, J.E. Antill, J. Nucl. Mater. 2 (1960) 194.

[32] D.R. McCracken, Atomic Energy of Canada Limited Report, AECL-8642, 1985.
[33] D.S. Cox, F.C. Iglesias, C.E.L. Hunt, R.D. Barrand, N.A. Keller, J.R. Mitchell, R.F. O'Connor, NUREG/CP-0078, 1987, p. 2.
[34] C.E.L. Hunt, D.S. Cox, Z. Liu, N.A. Keller, R.D. Barrand, R.F. O'Connor, F.C. Iglesias, in: Proceedings of the 12th Annual Canadian Nuclear Society Conference, Saskatoon, SK, June 1991, ISSN 0227-1907.
[35] D.R. Olander, J. Nucl. Mater. 252 (1998) 121.
[36] A.M. Anthony, R. Kiyoura, T. Sata, J. Nucl. Mater. 10 (1963) 8.
[37] T.B. Lindemer, T.M. Besmann, J. Nucl. Mater. 130 (1985) 473.
[38] B.V. Dobrov, V.V. Likhanskii, V.D. Ozrin, A.A. Solodov, M.P. Kissane, H. Manenc, J. Nucl. Mater. 255 (1998) 59.
[39] D.S. Cox, C.E.L. Hunt, Z. Liu, N.A. Keller, R.D. Barrand, R.F. O'Connor, in: Proceedings of the ANS Symposium on Safety of Nuclear Reactors, Portland, OR, July 1991, also AECL-10438.
[40] P. Ruello, G. Chirlesan, G. Petot-Ervas, C. Petot, L. Desgranges, J. Nucl. Mater. 325 (2004) 202.
[41] A.H. Booth, Atomic Energy of Canada Limited Report, AECL-496, 1957.
[42] D.S. Cox, C.E.L. Hunt, Z. Liu, F.C. Iglesias, N.A. Keller, R.D. Barrand, R.F. O'Connor, in: Proceedings of the 12th Annual Canadian Nuclear Society Conference, Saskatoon, SK, June 1991, ISSN 0227-1907.